The retinoic acid-metabolizing enzyme, CYP26A1, is essential for normal hindbrain patterning, vertebral identity, and development of posterior structures

Suzan Abu-Abed,[1,3] Pascal Dollé,[2,3] Daniel Metzger,[2] Barbara Beckett,[1] Pierre Chambon,[2] and Martin Petkovich[1,4]

[1]Cancer Research Labs, Queen's University, Kingston, Ontario, K7L 3N6, Canada; [2]Institut de Génétique et de Biologie Moléculaire et Cellulaire, CNRS/INSERM/ULP, Collège de France, BP 163-67404 Illkirch Cedex, CU de Strasbourg, France

The active derivative of vitamin A, retinoic acid (RA), is essential for normal embryonic development. The spatio-temporal distribution of embryonic RA results from regulated expression of RA-synthesizing retinaldehyde dehydrogenases and RA-metabolizing cytochrome P450s (CYP26). Excess RA administration or RA deficiency results in a complex spectrum of embryonic abnormalities. As a first step in understanding the developmental function of RA-metabolizing enzymes, we have disrupted the murine *Cyp26A1* gene. We report that *Cyp26A1*-null mutants die during mid-late gestation and show a number of major morphogenetic defects. Spina bifida and truncation of the tail and lumbosacral region (including abnormalities of the kidneys, urogenital tract, and hindgut) are the most conspicuous defects, leading in extreme cases to a sirenomelia ("mermaid tail") phenotype. *Cyp26A1* mutants also show posterior transformations of cervical vertebrae and abnormal patterning of the rostral hindbrain, which appears to be partially posteriorly transformed. These defects correlate with two major sites of *Cyp26A1* expression in the rostral neural plate and embryonic tail bud. Because all of the *Cyp26A1*$^{-/-}$ abnormalities closely resemble RA teratogenic effects, we postulate that the key function of CYP26A1 is to maintain specific embryonic areas in a RA-depleted state, to protect them against the deleterious effect of ectopic RA signaling.

[*Key Words*: Antero-posterior patterning; cytochrome P450; hindbrain; homeotic transformations; retinoids; teratogenesis]

Received September 27, 2000; revised version accepted December 6, 2000.

Retinoic acid (RA) is a key determinant of vertebrate embryo patterning and organogenesis (Hofmann and Eichele 1994; Ross et al. 2000 and references therein). RA action is temporally and spatially restricted to specific regions of the embryo because of the localized synthesis and degradation of RA. Two families of nuclear receptors (RARα, β, and γ and RXRα, β, and γ) that act as heterodimers transduce retinoid signals (Chambon 1996 and references therein). Knockouts of these nuclear receptors either alone or in combination have revealed functional roles for RAR and RXR isotypes; although single knockouts result in mild or no phenotypic changes, compound deletions closely phenocopy defects of fetal vitamin A deficiency (VAD) syndrome (Mendelsohn et al. 1994; Kastner et al. 1997; Mascrez et al. 1998; and references therein).

Studies of VAD and RA deficiency, as well as RA excess, support the view that the tissue distribution of RA is finely controlled. Vitamin A and RA deficiencies cause embryonic malformations that include abnormal eye, brain, heart, somite, and limb development (Morriss-Kay and Sokolova 1996; Niederreither et al. 1999, 2000; White et al. 2000b). Excess RA can also cause severe malformations, the nature of which depends on timing and dose of exposure. Exposure to RA during formation of the antero-posterior body axis (E7–7.8) results in posteriorizing homeotic transformations along the length of the vertebral column. Conversely, excess RA during the formation of posterior body structures results in anteriorizing homeotic transformations, including the appearance of supernumary ribs and caudally shifted os sacrum (Kessel 1992). Limb malformations are also observed in RA excess (Kochhar 1973), as are defects in craniofacial (Morriss-Kay and Sokolova 1996) and heart development (Chazaud et al. 1999), resulting in part from perturbed neural crest development. Some of these defects have

[3]These authors contributed equally to this work.
[4]Corresponding author.
E-MAIL petkovic@post.queensu.ca; FAX (613) 533-6830.
Article and publication are at www.genesdev.org/cgi/doi/10.1101/gad.855001.

been associated with altered temporal and spatial expression of RA regulated genes, notably the *Hox* genes. For example, ectopic *Hox* gene expression in the hindbrain of E7.5 RA-treated embryos indicates transformation of rhombomeres (r)2/3 to r4/5 identity (Conlon 1995 and references therein). Both *Hox* and *RAR* loss-of-function mutants show anterior vertebral homeotic transformations that are the counterpart of those observed in embryos exposed to RA excess or in which *Hox* genes have been overexpressed (Kessel and Gruss 1991; Krumlauf 1994; Lohnes et al. 1993, 1994).

The identification and cloning of retinaldehyde dehydrogenases involved in the production of RA from retinaldehyde (ALDH1, RALDH2, and RALDH3; Duester 2000 and references therein) and of cytochrome P450 enzymes involved in the inactivation of RA by conversion to 4-oxo- and 4-hydroxy-RA (cytochrome P450RAI-1 [CYP26A1]; White et al. 1996, 1997; Fujii et al. 1997; Ray et al. 1997; Abu-Abed et al. 1998; and cytochrome P450RAI-2 [CYP26B1]; White et al. 2000b) has provided important tools to map domains of embryonic RA synthesis and catabolism. *Raldh2* and *Cyp26A1* are expressed in nonoverlapping domains in the chick embryo (Swindell et al. 1999). Complementary expression patterns are also observed during caudal development in chick and mouse embryos, because *Raldh2* expression is predominant in somitic, presomitic, and lateral plate mesoderm except in the tail bud (Niederreither et al. 1997), whereas *Cyp26A1* expression is specific to tailbud tissues (Fujii et al. 1997; Iulianella et al. 1999). Expression of *Raldh2* and *Cyp26A1* in developing limbs of chick (Swindell et al. 1999) or mouse (Fujii et al. 1997) can be seen in proximal mesoderm and distal ectoderm, respectively. Complementary domains of *Raldh2*, *Aldh1*, and *Cyp26A1* expression have also been observed in developing retina (McCaffery et al. 1999) and heart (Moss et al. 1998). Consistent with expression data, regions expressing *Raldh2* produce RA and those expressing *Cyp26A1* degrade it. This has been shown by studying RA-responsive transgene activity (Mendelsohn et al. 1991; Rossant et al. 1991; Fujii et al. 1997; Niederreither et al. 1997; Maden et al. 1998) and biochemical analyses of RA synthesis and catabolic activity in embryonic explants (Iulianella et al. 1999; Swindell et al. 1999).

Targeted disruption of the *Raldh2* gene results in major developmental defects including shortening of the antero-posterior axis, incomplete neural tube closure, defective heart morphogenesis, limb bud deficiency, and hindbrain alterations, leading to mid-gestational death (Niederreither et al. 1999). RA could not be detected in these knockout embryos by using RA-responsive transgenes, with the exception of developing retina. Moreover, *Hox* genes known to be primary targets of RA were abnormally regulated in *Raldh2*-deficient embryos (Niederreither et al. 2000).

To define the role of CYP26A1 in generating localized distributions of RA, we have used homologous recombination to disrupt the mouse *Cyp26A1* gene. CYP26A1 loss-of-function mutants die before birth and show a spectrum of abnormalities reminiscent of RA excess teratogenesis, including exencephaly, spina bifida, posterior body truncations leading in most severe cases to hindlimb fusion (sirenomelia), posterior vertebral transformations, and partial transformation of the anterior hindbrain toward a more posterior identity. These data support a role for CYP26A1 in clearing RA from specific embryonic areas to protect them against inappropriate RA signaling.

Results

Generation of Cyp26A1*-deficient mice*

The *Cyp26A1* gene was disrupted by introducing a "floxed" (*loxP*-containing) targeted construct into *129/Sv* embryonic stem (ES) cells (Fig. 1A). Homologous recombination was identified in 20 of 280 G418-resistant ES cell clones by using probes flanking the 5′ and 3′ ends of the gene replacement construct shown in Figure 1 (data not shown). One positive clone was used for blastocyst injections, from which four chimeric males were generated (Dierich and Dollé 1997). Germ-line transmission of the floxed allele (L3) was observed with two of the chimeric males, whose male offspring were mated with females expressing Cre recombinase (Dupe et al. 1997).

Cyp26A1$^{-/+}$ mutants were obtained at the expected frequency in the progeny of Cre-excised mice and appeared fully viable. However, no living homozygous null (*Cyp26A1*$^{-/-}$) mutants could be identified in the progeny of *Cyp26A1*$^{-/+}$ intercrosses (314 animals analyzed). Litters from heterozygous intercrosses were collected at various stages and yolk sac DNA was PCR analyzed (Fig. 1C). The appearance of resorption sites, or partly degraded embryos at embryonic day (E) 11.5 and later stages indicated that the homozygous null mutants die during mid-late gestation, which was confirmed by DNA genotyping (data not shown).

Posterior truncation and sirenomelia

Two *Cyp26A1*$^{-/-}$ mutants recovered at E18.5 (of 39 conceptuses) showed striking, although distinct, abnormalities (Fig. 2). One had severe truncation of its entire posterior body (Fig. 2, cf. A and B), as well as spina bifida (lack of closure of posterior neural tube; Fig. 2B) and abdominoschisis (Fig. 2C). Its hindlimbs were abnormally twisted toward the left, but otherwise had normal size and digit number (Fig. 2C). The other mutant had a normally closed abdominal wall (Fig. 2D), but showed sirenomelia, that is, a mermaid-like tail resulting from complete fusion of the two hindlimbs to form an abnormal, two-digit structure (Fig. 2D,E). A small tissue outgrowth at the base of the sirenomelic limbs may represent a genuine tail rudiment (Fig. 2D; see also Fig. 3D).

Analysis of E13.5–14.5 *Cyp26A1*$^{-/-}$ mutants consistently revealed an abnormal posterior phenotype that

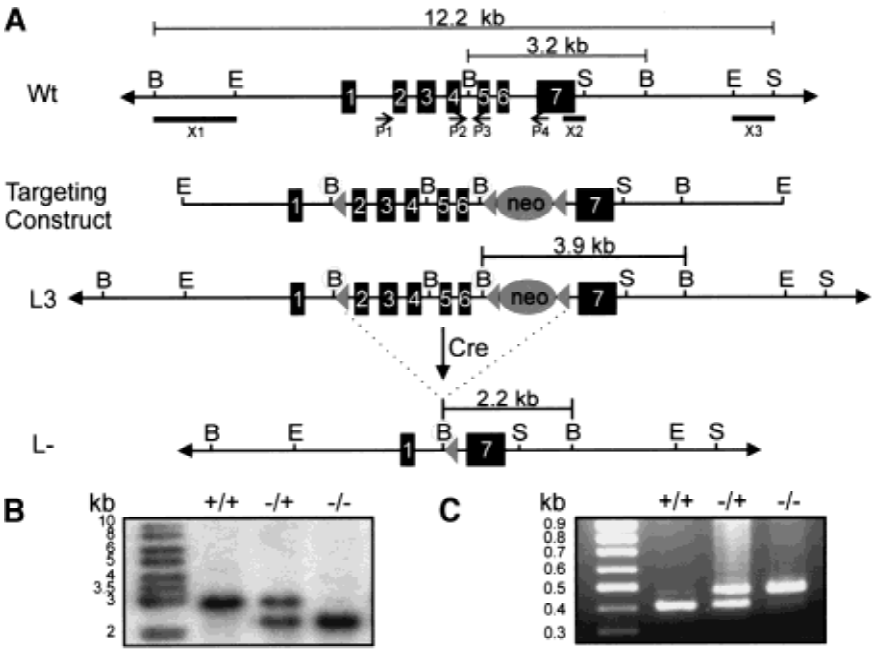

Figure 1. Targetted excision of exons 2–6 of the *Cyp26A1* locus by using the Cre-*loxP* system. (*A*) Schematic representation of the *Cyp26A1* wild-type locus (Wt, *top*), targeting construct (*middle*), targeted allele (L3, *middle*), and null allele (L–, *bottom*). Exons are represented by solid rectangles. The targeting construct is flanked by 2.8 kb of 5′ homology and 4.3 kb of 3′ homology and contains novel 5′ *Bgl*II restriction sites preceding the subcloned antisense *loxP* sites (solid triangle) and PGK-neo cassette (also flanked by *loxP* sites) in introns 1 and 6, respectively. (*B*) Southern blot analysis of yolk sac genomic DNA of progeny from *Cyp26A1*$^{L-/+}$ matings by using a *Bgl*II digest. Cre-mediated excision of exons 2–6 was verified by using a 565-bp probe that hybridizes to a 3.2- and 2.2-kb fragment in the case of the wild-type (WT or +) and deleted alleles (L– or –), respectively. (*C*) PCR analysis of yolk sac genomic DNA. Four primers (P1–P4) used for PCR identification of the *Cyp26A1* alleles are indicated by arrows below the Wt locus. P1 and P4 amplify a 484-bp fragment from the null allele (–), whereas P2 and P3 amplify a 414-bp fragment from the WT allele (+). (B) *Bgl*II; (E) *Eco*RI; (encircled B) newly created *Bgl*II site; (S) *Ssp*I. Note that not all *Bgl*II and *Ssp*I restriction sites are shown.

was, however, variable in its expressivity. Most of the mutants had a more or less severely truncated tail, usually associated with spina bifida (Fig. 3B). The hindlimbs were fully separated, and the genital tubercle was present (Fig. 3B). More severely affected *Cyp26A1*$^{-/-}$ fetuses lacked both a tail rudiment and genital tubercle, and had malpositioned hindlimbs (Fig. 3C). Sirenomelia (Fig. 3D), was observed only in 20% (3/15) of the mutant fetuses. No additional limb defects could be detected in *Cyp26A1*$^{-/-}$ fetuses that did not show sirenomelia (Fig. 3B–D; see also Fig. 2B,C). Some of the *Cyp26A1*$^{-/-}$ fetuses showed exencephaly (Fig. 3E), whereas other cra-

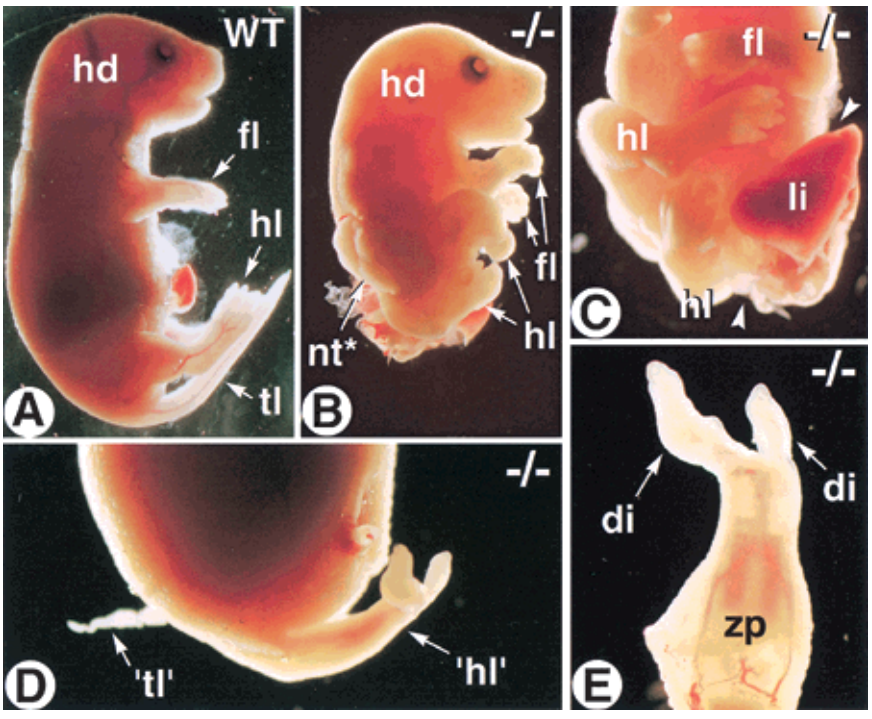

Figure 2. Morphological abnormalities of E18.5 *Cyp26A1*$^{-/-}$ fetuses. Profile views of wild-type (WT) (*A*) and *Cyp26A1*$^{-/-}$ (*B*) littermates. (*C*) Posterior body region of the same mutant. Arrowheads indicate the open abdominal wall, with protruding viscera. (*D*) Profile view of the abnormal caudal region of a second *Cyp26A1*$^{-/-}$ mutant. (*E*) Detail of the abnormal sirenomelic hindlimb ('hl'). (di) digit; (hd) head; (fl) forelimb; (hl) hindlimb; (li) liver; (nt*) open neural tube (spina bifida); (tl) tail; ('tl') abnormal tail rudiment; (zp) zeugopod.

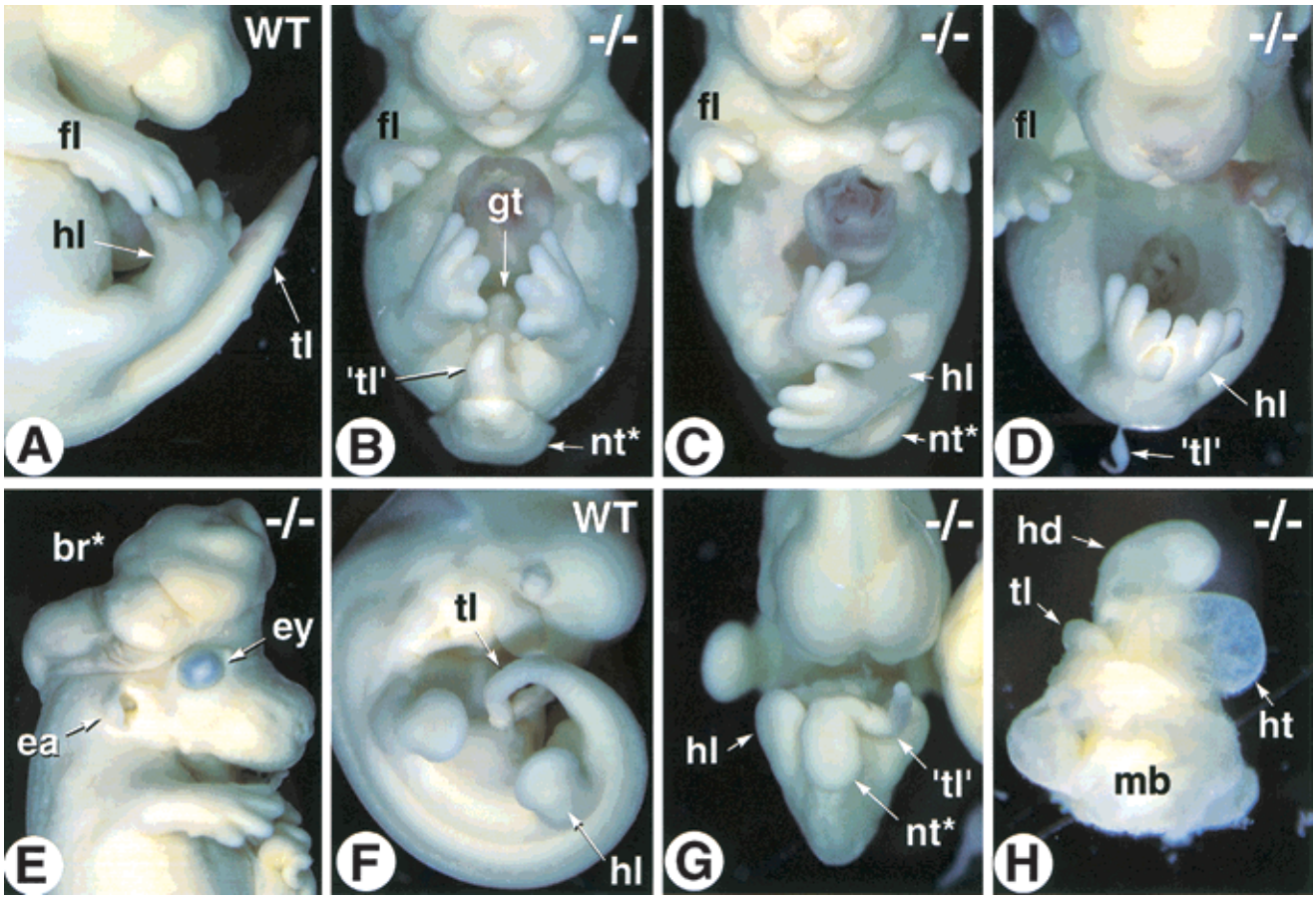

Figure 3. Variability of the *Cyp26A1*$^{-/-}$ phenotype. (*A*) Close-up of the caudal region of an E14.5 wild-type (WT) embryo (profile view). (*B–D*) E14.5 *Cyp26A1*$^{-/-}$ embryos with increasing degrees of caudal truncation and hindlimb malposition and malformations (frontal views). (*E*) E13.5 *Cyp26A1*$^{-/-}$ embryo with exencephaly. (*F,G*) Abnormal twisting of the tail bud and opening of the neural tube in an E10.5 *Cyp26A1*$^{-/-}$ embryo (*G*, compare with WT littermate, *F*). (*H*) E10.5 *Cyp26A1*$^{-/-}$ mutant showing arrested development at a stage equivalent to WT E8.5 (before embryonic turning) and a markedly dilated heart tube. (br*) exencephalic brain tissue; (ea) ear; (ey) eye; (gt) genital tubercle; (hd) head; (ht) heart; (fl) forelimb; (hl) hindlimb; (mb) extraembryonic membranes; (nt*) open neural tube; (tl) tail; ('tl') tail rudiment.

niofacial structures (including eyes and ears, which express *Cyp26A1* during development) appeared normal (Fig. 3E and data not shown).

Embryos were also collected at earlier developmental stages (E9.5–11.5). The tail rudiment of *Cyp26A1*$^{-/-}$ embryos always appeared more or less severely twisted and truncated (Fig. 3, cf. F and G). Some of the mutants were developmentally arrested at approximately E8.5–9.5 and showed dilated heart cavity (Fig. 3H), or pericardial ballooning with imperfectly looped heart tube (data not shown), indicating that improper cardiovascular development could explain the early lethality of some of the *Cyp26A1*$^{-/-}$ mutants.

Abnormal development of the posterior gut and urogenital system

Several *Cyp26A1*$^{-/-}$ mutants were analyzed histologically at E13.5–14.5. "Mildly" affected fetuses (e.g., Fig. 3B) had their kidneys fused at their posterior extremities ("horseshoe kidney": Fig. 4, cf. A and B). The gonads were separated, but the mesonephric and paramesonephric ducts (genital tract precursors) prematurely merged within a hypoplastic urogenital sinus (Fig. 4D,E). Furthermore, the hindgut ended as a blind ampulla within the wall of the abnormal urogenital sinus (Fig. 4E, arrowheads). Thus, the caudal portion of the hindgut (presumptive rectum) was absent in *Cyp26A1*$^{-/-}$ mutants (Fig. 4D,E). The genital tubercle was present, although hypoplastic and with a poorly developed urethral groove (Fig. 4H). The tail rudiment of these fetuses was mostly composed of disorganized neural tissue (Fig. 4H).

Histological analysis of a sirenomelic fetus revealed a single, medial kidney located between the two gonads (Fig. 4C). Interestingly, the second rudimentary kidney, consisting of only a few metanephric tubules, was found ectopically between the hindlimb cartilages and neural tube (Fig. 4F). The urogenital ducts and ureter buds

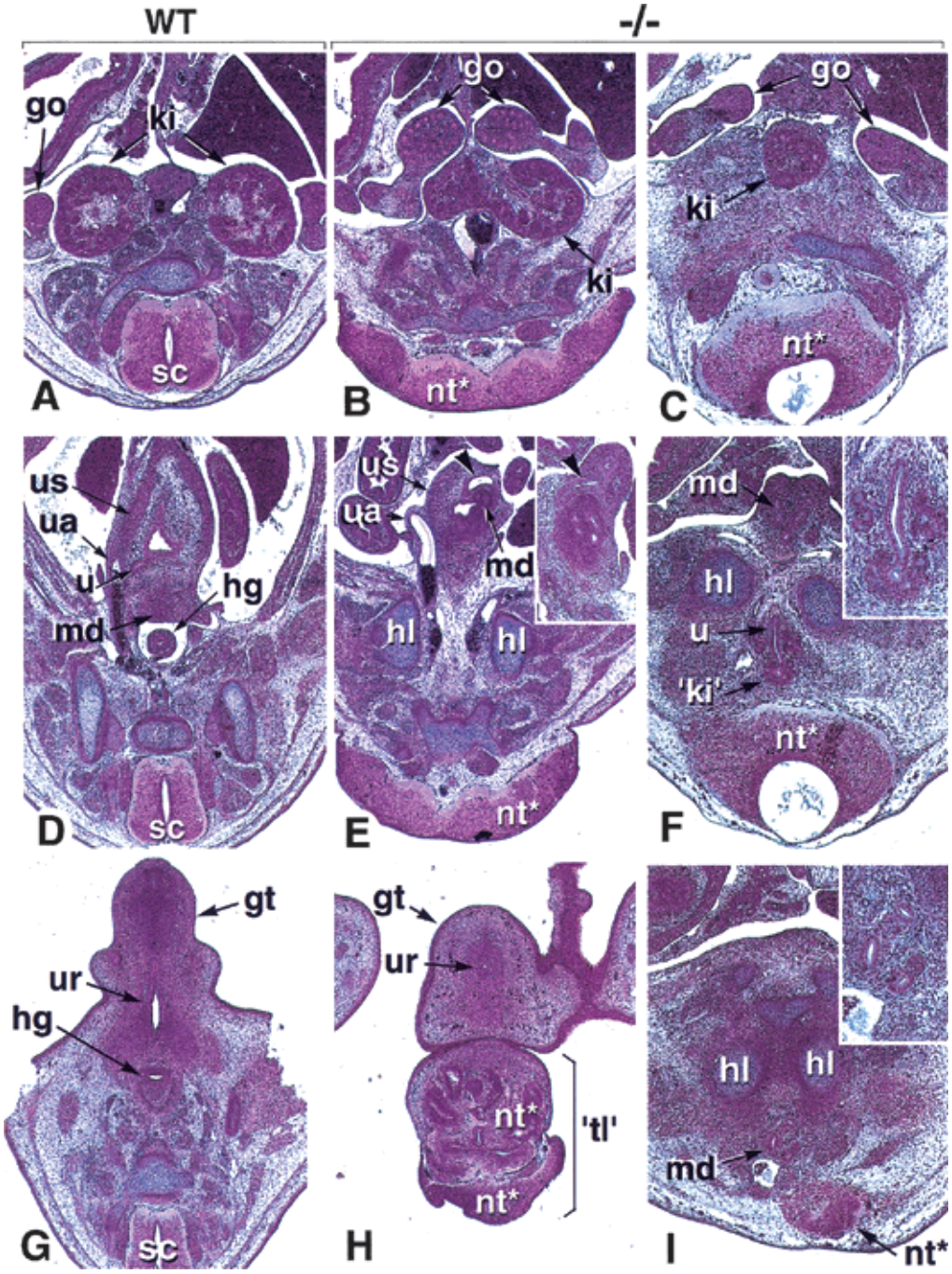

Figure 4. Histological defects of *Cyp26A1*$^{-/-}$ embryos. Three successive section planes are shown, at the level of the kidneys (*A–C*), urogenital sinus (developing urinary bladder; *D–F*), and genital tubercle (*G–I*). (*A*,*D*,*G*) E14.5 control embryo. (*B*,*E*,H) E14.5 *Cyp26A1*$^{-/-}$ embryo with a 'mild' (nonsirenomelic) phenotype. (*C*,*F*,*I*) E13.5 *Cyp26A1*$^{-/-}$ embryo with sirenomelic hindlimbs. Panel *E* and its inset shows the intra-abdominal ending of the hindgut as a dilated ampulla within the urogenital sinus wall (arrowheads). Panel *F* and *I* insets are higher magnifications of the abnormal kidney rudiment and mesonephric ducts, respectively. (go) gonad; (gt) genital tubercle; (hg) hindgut; (hl) hindlimb; (ki) kidney; (md) mesonephric ducts; (nt*) abnormal neural tissue; (sc) spinal cord; ('tl') abnormal tail; (ua) umbilical artery; (u) ureter; (ur) urethral groove; (us) urogenital sinus.

ended blindly below the sirenomelic limbs, without any evidence of a urogenital sinus (Fig. 4I), whereas the hindgut ended blindly in the abdominal cavity (not shown). Thus, morphogenesis of the terminal portion of the urogenital system is more or less severely impaired in *Cyp26A1*$^{-/-}$ mutants, whereas the terminal portion of the gut is consistently lacking. Other internal organs appeared normal (data not shown).

Vertebral transformations

Alcian blue stainings, performed at E14.5 to characterize the tail and hindlimb defects of *Cyp26A1*$^{-/-}$ mutants, revealed transformations of cervical vertebrae (Fig. 5). The wild-type (WT) vertebral formula consists of 7 cervical (C1–C7), 13 thoracic (T1–T13), 6 lumbar (L1–L6), 4 sacral, and a variable number of caudal vertebrae (Kessel and Gruss 1991). In some of the *Cyp26A1*$^{-/-}$ mutants, the spinous process of C1 was split into two parts, its caudal portion resembling the spinous processes of more posterior cervical vertebrae (Fig. 5B, arrow). Other *Cyp26A1*$^{-/-}$ fetuses had a normal C1 vertebra, but the spinous process of C2 was abnormally split into two branches (Fig. 5C, arrows). The mutant C7 vertebra consistently harbored a full pair of ribs, indicating a thoracic-like transformation (Fig. 5, cf. A and B–D). The anterior tuberculum normally found on C6 in wild-type embryos (Fig. 1A, bracket) was found on C5 in *Cyp26A1*$^{-/-}$ mutants (Fig. 5B,D, brackets), indicating a posterior transformation of C5 and C6. Abnormal rib fusions were occasionally seen (Fig. 5D).

In wild-type embryos, the first 7 pairs of ribs articulate with the sternum (vertebrosternal ribs) (Fig. 5E). *Cyp26A1*$^{-/-}$mutants had 8 pairs of vertebrosternal ribs (including the supernumerary ribs on C7; Fig. 5F), indicating that T7 and T8 are not posteriorly transformed. Likewise, a total of 14 pairs of ribs were present in mutants (Fig. 5F), indicating that T13 is not transformed. Thus, the posterior transformations do not seem to extend along the thoracic vertebrae of *Cyp26A1*$^{-/-}$ mutants.

Vertebral cartilage elements were highly abnormal caudal to L1, and the tail rudiment of *Cyp26A1*$^{-/-}$ fetuses contained a small number of ill-defined vertebral condensations (Fig. 5G,H). In severely affected mutants,

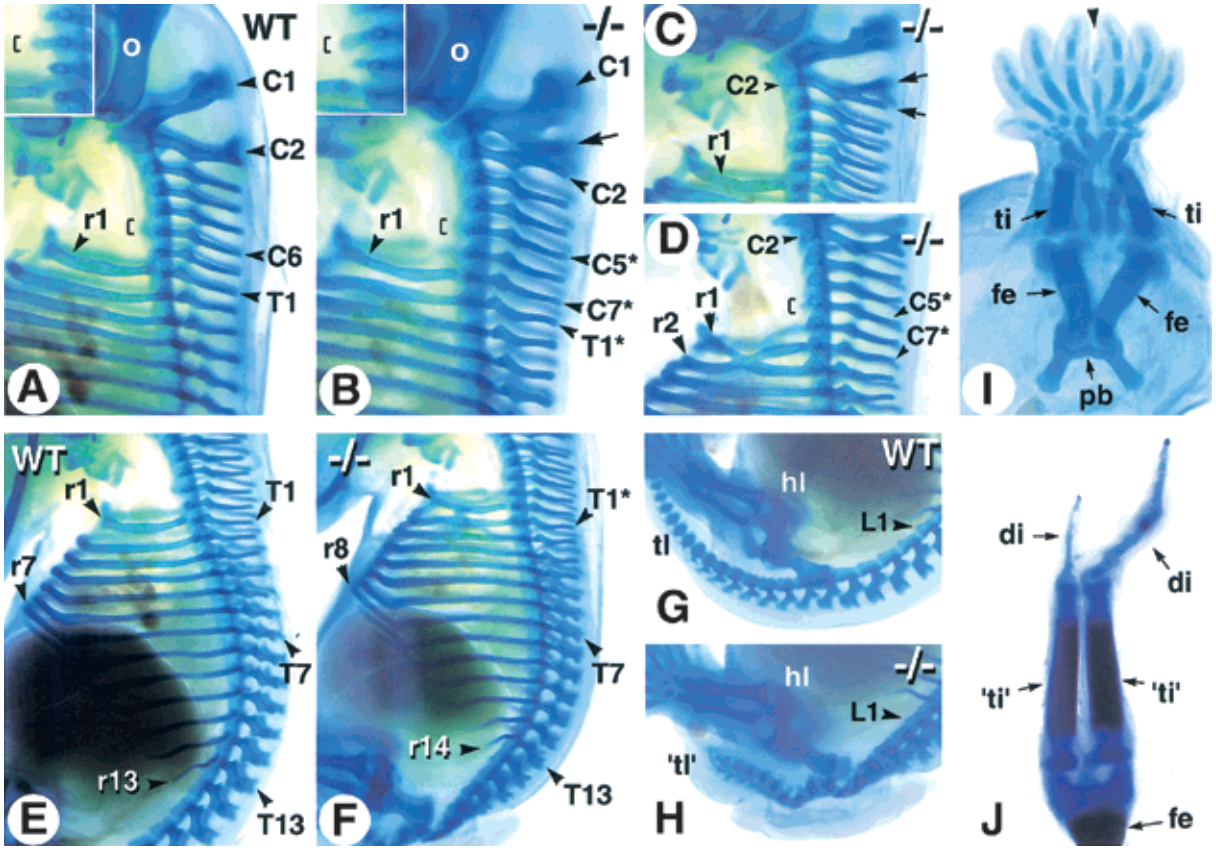

Figure 5. Skeletal defects of *Cyp26A1*$^{-/-}$ mutants. Whole-mount alcian blue cartilage stainings were performed at E14.5. (*A,E,G*) Profile views of the cervical (*A*), thoracic (*E*), and lumbosacral (*G*) region of control embryos. (*B–D*) Abnormal patterning of the cervical and upper thoracic vertebrae in *Cyp26A1*$^{-/-}$ mutants. Insets in (*A*) and (*B*) are close-ups focused on the tuberculum anterior (brackets), which is a characteristic structure of C6 in wild-type embryos. The arrow in (*B*) points to a supernumerary spinous process on C1. In *C*, such a supernumerary process is branched on C2 (arrows). (*F*) Except for the presence of a supernumerary rib on C7, the mutant rib cage appears normally patterned. (*H*) Disorganized and poorly differentiated vertebral cartilages in a *Cyp26A1*$^{-/-}$ embryo, caudally to the first lumbar (L1) vertebra. Note, however, the normal position and pattern of the hindlimb. (*I*) Partial fusion of skeletal elements in the sirenomelic hindlimbs of an E13.5 *Cyp26A1*$^{-/-}$ embryo. (*J*) Skeletal pattern of the rudimentary "hindlimbs" of the E18.5 mutant shown in Figure 2, D and E. (C1–C7) cervical vertebrae; (di) digit; (fe) femur; (hl) hindlimb; (pb) pelvic bone; (r1–r14) ribs; (T1–T13) thoracic vertebrae; (L1) first lumbar vertebra; (ti) tibia. The mutant vertebrae have been numbered according to the wild-type formula, and transformed vertebrae are indicated by asterisks.

the vertebral column was truncated caudal to L1 (data not shown). Sirenomelic hindlimbs were linked to a single floating pelvic bone rudiment and consisted of symmetrically arranged femoral, zeugopodal (tibia and fibula), and autopodal (tarsal and digit) cartilage elements sharing a common "posterior" digit (Fig. 5I, arrowhead). The most severe case (Fig. 2E) consisted of a single femur, two tibia-like bones, each connecting to a single digit (including a hypoplastic one) (Fig. 5J). The cartilaginous patterns of nonsirenomelic hindlimbs, as well as those of all forelimbs, were normal in *Cyp26A1*$^{-/-}$ mutants (Fig. 5H, and data not shown).

Molecular characterization of the caudal regression phenotype

Two molecular markers of tail-bud development were analyzed at E8.5 and E9.5 (Fig. 6). *Brachyury* gene transcripts are expressed in both tail-bud mesoderm and neuroepithelium, and in the notochord (Fig. 6A,C; Wilkinson et al. 1990). *Brachyury* was expressed at normal levels in the caudal region of *Cyp26A1*$^{-/-}$ embryos, but its expression domain was spatially reduced (Fig. 6, cf. A and B). In addition, the caudal-most portion of the notochord ("chordoneural hinge") was abnormally curved and/or bifurcated in *Cyp26A1*$^{-/-}$ embryos (Fig. 6B). E9.5 mutant embryos still showed marked notochordal deformation (Fig. 6D). In addition, *Brachyury* transcripts were only detected in the dorsal (neuroepithelial) portion of the mutant tailbud, indicating a defect in tailbud mesoderm formation (Fig. 6D). We also analyzed expression of *Wnt3A* because (1) loss of function of this gene leads to posterior truncations (Takada et al. 1994), somewhat similar to those of *Cyp26A1*$^{-/-}$ mutants, and (2) *Wnt3A* expression was found to be down-regulated on administration of excess RA (Shum et al. 1999). *Wnt3A* expression was present in *Cyp26A1*$^{-/-}$ embryos, but its spatial distribution was abnormally restricted toward the midline of the posterior neural plate (Fig. 6, cf. E and F).

Shum et al. (1999) reported abnormal apoptosis of tailbud cells following excess RA administration. Therefore, we used the TUNEL technique to analyze apoptosis in

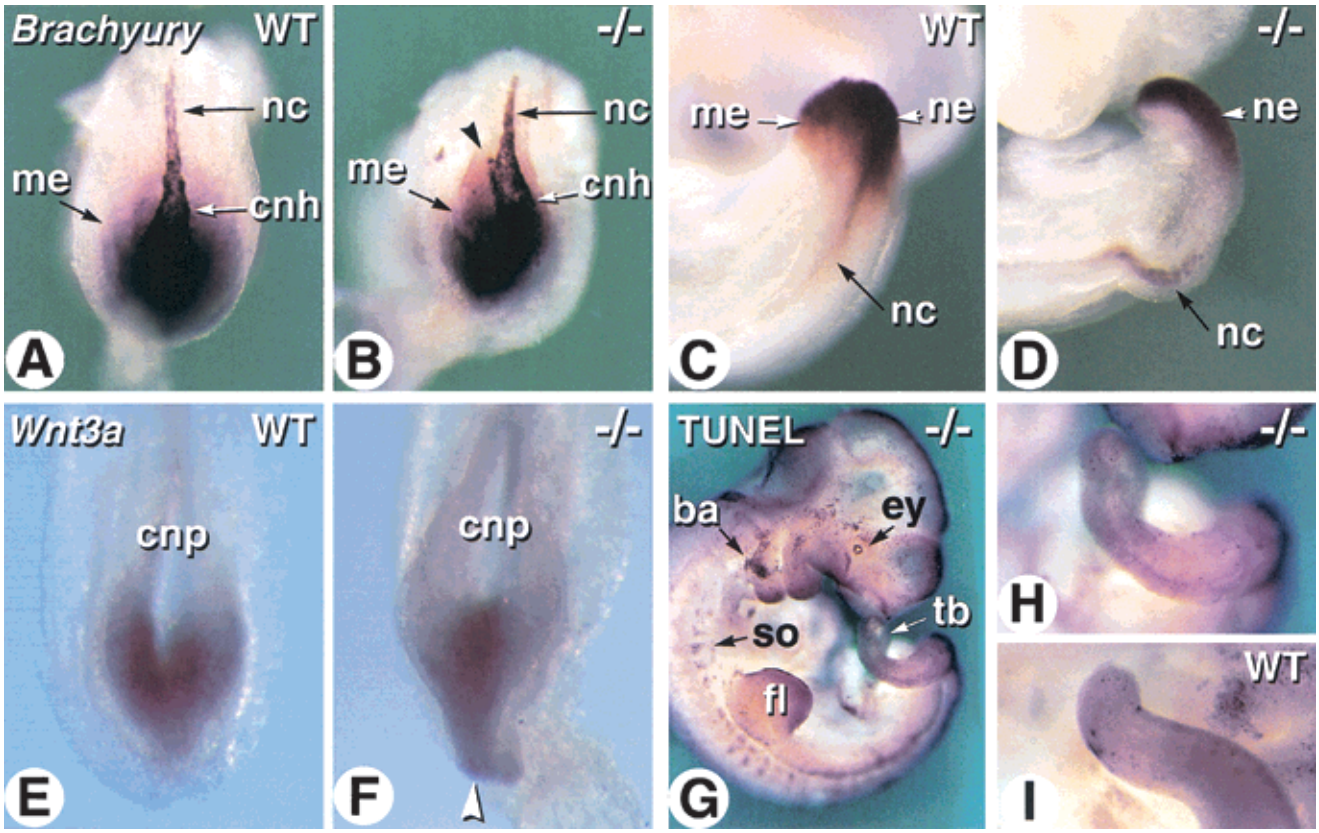

Figure 6. Molecular analysis of tail development in *Cyp26A1*$^{-/-}$ embryos. (*A–D*) Whole-mount in situ hybridization of *Brachyury* transcripts in wild-type (WT) (*A,C*) and *Cyp26A1*$^{-/-}$ (*B,D*) embryos. *A,B* are dorsal views of the caudal extremity of E8.5 embryos. Arrowhead in *B* shows abnormal bifurcation of the caudal portion of the notochord. *C,D* are views of the tail bud of E9.5 embryos. (*E,F*) Comparison of *Wnt3a* transcript distribution in the caudal neural plate of E8.5 WT (*E*) and *Cyp26A1*$^{-/-}$ (*F*) embryos. The arrowhead points to the abnormally thin caudal extremity of the neuroepithelium in the mutant embryo. (*G*) TUNEL labeling of an E10.5 *Cyp26A1*$^{-/-}$ embryo. (*H,I*) comparative views of the tail buds of the same mutant (*H*) and a littermate control (*I*). (ba) branchial arch; (cnh) chordoneural hinge; (cnp) caudal neural plate; (ey) eye; (fl) forelimb bud; (me) caudal/tail-bud mesoderm; (nc) notochord; (ne) tail-bud neuroepithelium; (so) somites; (tb) tail bud.

Cyp26A1$^{-/-}$ mutants. At E9.5 (data not shown) and E10.5 (Fig. 6G,H), *Cyp26A1*$^{-/-}$ embryos showed the previously described physiological pattern of cell death (Conlon et al. 1995), for example, in the eye, branchial arch mesenchyme, somites, or limb bud apical ectodermal ridge (AER) (Fig. 6G), but no significant increase in apoptosis was detected in the tail bud (Fig. 6G). Few scattered TUNEL-labeled cells were detected in the mutant tail mesenchyme (Fig. 6H), similar to control tail buds (Fig. 6I).

Abnormalities of the anterior hindbrain

Embryonic RA controls growth and patterning of the posterior hindbrain region (Gale et al. 1999; Maden 1999; Niederreither et al. 2000). *Cyp26A1* is specifically expressed in developing r2 (Fig. 7A; Fujii et al. 1997), indicating that development of this rhombomere and/or of the rostral hindbrain region requires localized RA metabolism. Histological analysis at E9.5 (data not shown) and E10.5 (Fig. 7B) revealed the presence of evenly spaced rhombomeric bulges, indicating that there is no major growth or segmentation defect in the *Cyp26A1*$^{-/-}$ hindbrain. We analyzed *Krox20* gene transcripts as markers for r3 and r5 (Fig. 7C; Schneider-Maunoury et al. 1993). These rhombomere territories were well-defined in *Cyp26A1*$^{-/-}$ mutants (Fig. 7D). However, the intervening (prospective r4) territory was larger than in wild-type embryos, and the r3 band contained patches of unlabeled cells (Fig. 7D, arrows). Analysis of *Hoxb1*, an RA-inducible r4-specific marker, confirmed the presence of an enlarged prospective r4 territory in some of the *Cyp26A1*$^{-/-}$ embryos (Fig. 7F,G). In addition, patches or stripes of cells ectopically expressing *Hoxb1* were found rostrally to the prospective r4 (Fig. 7F,G). Figure 7G shows a mu-

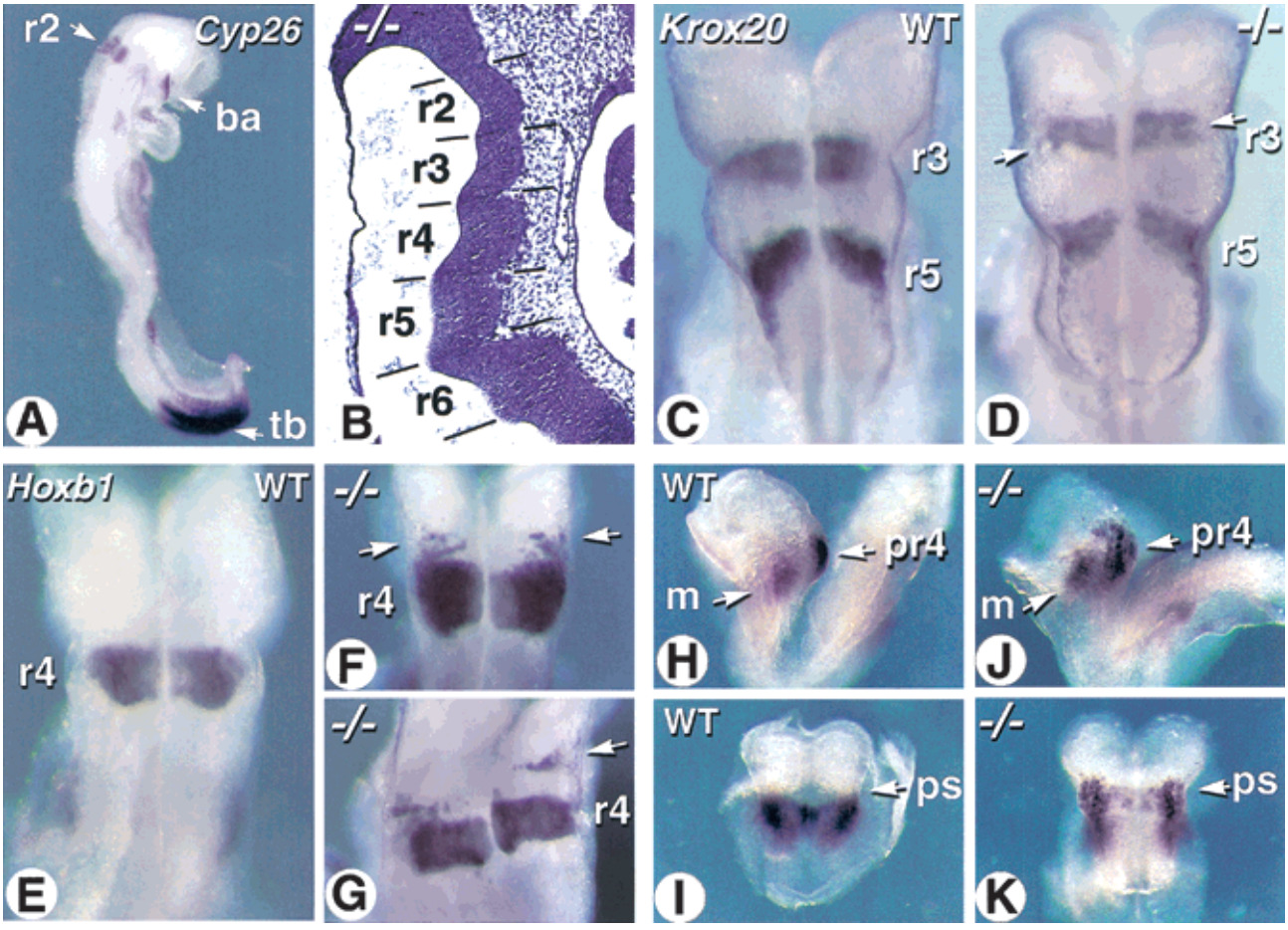

Figure 7. Abnormal patterning of the rostral hindbrain in *Cyp26A1*$^{-/-}$ embryos. (*A*) Expression pattern of *Cyp26A1* in a wild-type E8.5 embryo, detected by whole-mount in situ hybridization. (*B*) Sagittal section through the hindbrain region of an E9.5 *Cyp26A1*$^{-/-}$ embryo. Hematoxylin-eosin staining. (*C,D*) Whole-mount in situ hybridization of *Krox20* transcripts in E8.5 wild-type (WT) control (*C*) and *Cyp26A1*$^{-/-}$ (*D*) embryos. Dorsal views of the hindbrain region. Arrows point to patches of unlabeled cells in mutant r3. (*E–G*) *Hoxb1* transcript distribution in the hindbrain of E8.5 WT (*E*) and *Cyp26A1*$^{-/-}$ (*F,G*) embryos. Arrows show ectopic *Hoxb1* expression rostrally to r4 in mutants. (*H–K*) *EphA2* transcript distribution in E8.25 WT (*H,I*) and *Cyp26A1*$^{-/-}$ (*J,K*) embryos. Profile views (*H,J*) show the distinct *EphA2* expression domains in neuroepithelium and head mesenchyme, whereas dorsal views after removal of the caudal region show the hindbrain region (*I,K*). Note that *EphA2* transcripts extend beyond the preotic sulcus (ps) in the mutant embryo. (ba) branchial arch; (m) mesenchyme; (pr4) prospective rhombomere 4; (r2–r6) rhombomeres; (tb) tail bud.

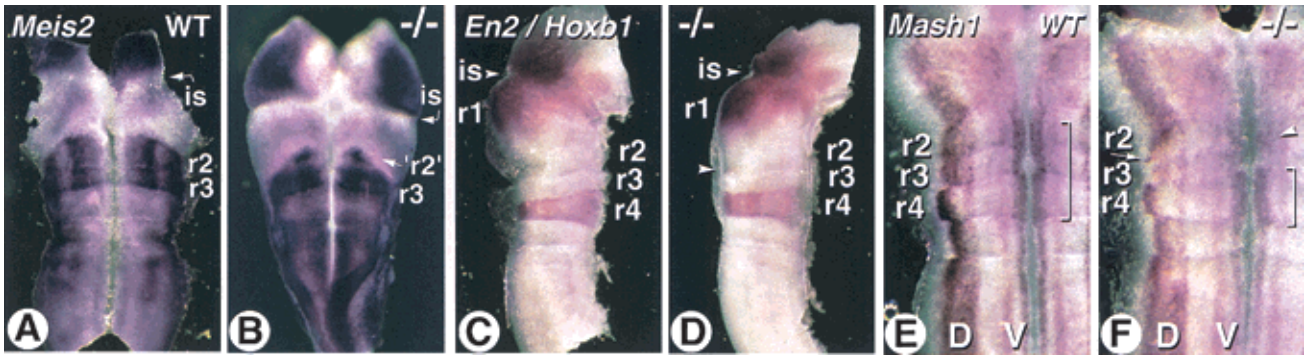

Figure 8. Molecular alterations in the *Cyp26A1*$^{-/-}$ rostral hindbrain. (*A,B*) Flatmounts of the mid-hindbrain region of E9.5 control (*A*) and *Cyp26A1*$^{-/-}$ (*B*) embryos hybridized with a *Meis2* probe. Note that this mutant embryo was exencephalic. (*C,D*) Double labeling with *Engrailed-2* (*En2*) and *Hoxb1* probes on E10.5 control (*C*) and mutant (*D*) embryos. The mid-hindbrain region was bisected and one of its halves is shown in flatmount (floor plate is oriented to the right). (*E,F*) Details of flatmounted hindbrains from E10.5 control (*E*) and *Cyp26A1*$^{-/-}$ (*F*) embryos hybridized with a *Mash1* probe. The specific distribution of *Mash1* transcripts in dorsal (D) and ventral (V) neuronal columns is thus seen. The bracket indicates more prominent ventral expression in wild-type (WT) rhombomeres 2–4. In the mutant, this ventral column is disrupted at the level of r3–r2, where only patches of cells show higher *Mash1* expression (arrowhead). The arrow points to ectopic dorsally located *Mash1*-expressing cells in the caudal portion of mutant r2. (is) rhombencephalic isthmus; (r1–r4) rhombomeres.

tant embryo in which an ectopic stripe of *Hoxb1*-expressing cells is separated from r4 by the width of a rhombomere, indicating that ectopic *Hoxb1* expression extends to part of the r2 territory. The *EphA2* receptor kinase gene, normally expressed in the prospective r4 domain before the onset of hindbrain segmentation (Fig. 7H,I; Xu et al. 1999), was expressed in a patchy manner, and expanded more rostrally in the hindbrain neuroepithelium of *Cyp26A1*$^{-/-}$ embryos (Fig. 7J,K). *EphA2* was, however, properly expressed in the head mesenchyme of *Cyp26A1*$^{-/-}$ embryos (Fig. 7J).

We next analyzed expression of the homeobox gene *Meis2* , which marks r2 and r3 (Oulad-Abdelghani et al. 1998) to confirm a possible change in r2–r3 identity in *Cyp26A1*$^{-/-}$ mutants. *Cyp26A1*$^{-/-}$ embryos showed a well-defined r3 band with high *Meis2* expression (Fig. 8B). However, only two small regions of ventral cells expressed *Meis2* in the putative r2 territory (Fig. 8B), thus supporting the conclusion that this rhombomere is abnormally specified in mutants. To assay for r1 fate, we used *Engrailed-2* (*En2*), whose expression extends on both sides of the rhombencephalic isthmus, that is, in prospective r1 and midbrain territories (Fig. 8C; Joyner 1996). *En2* transcript distribution was not altered in E10.5 *Cyp26A1*$^{-/-}$ mutants (Fig. 8D). In a double-labeling experiment with *Hoxb1*, the gap between *En2* and *Hoxb1* transcript domains was comparable in wild type and mutants (Fig. 8, cf. C and D). At this stage, most of *Hoxb1* ectopic expression had disappeared in mutants, except in a few dorsally located cells (Fig. 8D, arrowhead), but a subtle increase in r4 size was still detected (Fig. 8, cf. C and D).

To investigate whether these early patterning defects affect the organization of neuronal precursors, we next analyzed expression of *Mash1*, a "neurogenic" helix-loop-helix transcription factor (Guillemot and Joyner 1993) normally expressed along two ventral longitudinal columns and a broader dorsal column in the E10.5 wild-type hindbrain, with a distinct dorsal distribution in r4 (Fig. 8E; Davenne et al. 1999). *Mash1* transcript distribution was disorganized in r2–r3 of *Cyp26A1*$^{-/-}$ embryos (Fig. 8F). Both dorsal and ventral columns were interrupted and only contained scarce *Mash1*-expressing cells (Fig. 8F, arrowhead). In addition, some *Mash1*-expressing cells were found in an abnormal dorsal location in the caudal portion of r2, which mimicked the r4-specific transcript distribution (Fig. 8F, arrow). This further supports the conclusion of a partial posterior transformation of r2 into a r4-like identity.

To see whether these molecular alterations affect cranial nerve patterning, E10.5 embryos were immunostained with an antineurofilament antibody (Fig. 9). The vestibulo-cochlear and facial (n7) nerves both exit from r4 and their sensory cells are juxtaposed in a single facial-acoustic ganglion (g7–8, Fig. 9A). Both the morphology of the g7–8 ganglion and the trajectories of the n7 fibers were not detectably altered in *Cyp26A1*$^{-/-}$ embryos (Fig. 9B). Nerve tracts arising from more caudal hindbrain levels were also normal in mutants (e.g., the glossopharyngeal and vagus nerves, n9 and n10, in Fig. 9). In wild-type embryos, the trigeminal nerve (n5), which arises from r2 and r3 and exits the hindbrain at the level of r2, forms a large sensory ganglion (g5, Gasser's ganglion) and divides into three branches, the ophthalmic (n5o), maxillary (n5mx), and mandibular (n5md) nerves (Fig. 9A). The location of the n5 exit point, as well as the thickness of its axon bundle and the spacing with the facial-acoustic exit point (which corresponds to the width of r3) were not detectably abnormal in *Cyp26A1*$^{-/-}$ embryos (Fig. 9, cf. A and B). The trigeminal ganglion (g5) had a normal morphology, but its distal nerve fibers were abnormally patterned in mutants (Fig. 9B). Whereas the mandibular nerve (n5md) appeared normal, the branch corresponding to the developing maxillary nerve was abnormally wide

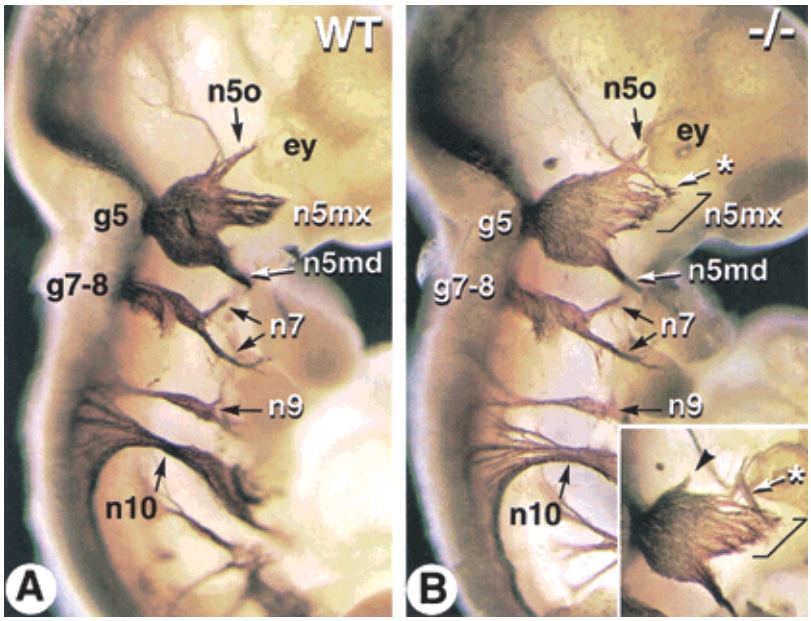

Figure 9. Abnormal trigeminal nerve patterning in *Cyp26A1*$^{-/-}$ embryos. Whole-mount immunostaining with an antineurofilament monoclonal antibody was performed on E10.5 wild-type (WT) (*A*) and *Cyp26A1*$^{-/-}$ (*B*) embryos. Neurofilament-labeled nerve tracts are visualized after partial removal of the surface ectoderm. An inset in (*B*) shows the contralateral trigeminal ganglion of the mutant embryo (in reverse orientation). Brackets indicate an enlarged maxillary nerve component in the mutant embryo. Asterisks point to abnormal routes of some putative ophthalmic nerve fibers, and an arrowhead points to a small ectopic rostral nerve tract. (ey) eye; (g5) trigeminal ganglion; (g7–8) facial-acoustic ganglia; (n5md/mx/o) mandibular, maxillary and ophthalmic branches of the trigeminal nerve; (n7) facial nerve branches; (n9) glossopharyngeal nerve; (n10) vagus nerve.

(Fig. 9B, bracket). In contrast, the ophthalmic nerve tract (n5o) was reduced, and part of its fibers were misrouted toward the maxillary branch (Fig. 9B, asterisk) and/or formed a small ectopic nerve tract (inset of Fig. 9B, arrowhead). We conclude that the *Cyp26A1*$^{-/-}$ r2–r3 molecular defects lead to abnormal patterning of their cranial nerve derivatives.

Discussion

RA signaling is crucial during normal morphogenesis and organogenesis. Here, we describe the phenotypic consequences of the genetic ablation of the RA-metabolizing enzyme CYP26A1. Our study, together with that of Sakai et al. (2001), who independently generated a *Cyp26A1*-null mutation, along with the recent analyses of *Raldh2*-null mutants (Niederreither et al. 1999, 2000; Sakai et al. 2001), strongly support the view that RA levels are tightly regulated in the embryo because of specific distributions of both RA-synthesizing and RA-metabolizing activities. However, our data do not fully support the notion that CYP26A1 participates in the generation of embryonic RA gradient(s), as hypothesized in the "morphogen" theory of RA function (Hofmann and Eichele 1994). Rather, we propose that the role of CYP26A1 is to confine the RA generated by RALDH2 and other RA-synthesizing enzymes.

Caudal defects in Cyp26A1 *mutants*

Development requires at least one functional *Cyp26A1* allele, because heterozygous mutants are fertile and do not show any obvious morphological defects. *Cyp26A1*$^{-/-}$ embryo mutants die sometimes as early as E9.5 and as late as E18.5 or at birth. The cause for this variability is not clear, but because all embryonic vitamin A is of maternal origin, there may be some variability in the delivery of vitamin A and/or RA by pregnant dams, which in turn could affect the levels of retinoids available to their conceptuses. Note in this respect that some of the phenotypic defects described by Sakai et al. (2001), although similar, appear to be more severe than in our present *Cyp26A1*$^{-/-}$ mice. This could result from differences in genetic backgrounds or from dietary retinoid levels provided to the animals.

At E8.5–9.5, *Cyp26A1* is expressed in the various components of the tail bud, that is, in the neural plate caudal to the posterior neuropore, the hindgut endoderm, and the tail-bud mesoderm (Fujii et al. 1997; Iulianella et al. 1999). *Cyp26A1*$^{-/-}$ mutants show severe defects in the development of posterior structures, which are strikingly similar to excess RA teratogenic effects. Spina bifida, agenesis of the tail, caudal vertebral defects, rectal agenesis, kidney malformations, abdominoschisis, and sirenomelia (mermaid syndrome) are defects similar to those due to RA excess during gastrulation (Kessel and Gruss 1991; Padmanabhan 1998). The development of disorganized neural tissue outgrowths within truncated tail rudiments is also common to *Cyp26A1*$^{-/-}$ (this study) and RA-treated (Shum et al. 1999) mouse embryos. The most severe *Cyp26A1*$^{-/-}$ caudal regression consists of complete lumbosacral truncation up to the level of L1, similar to the effect of a teratogenic excess of RA at E8.5–9 (Lohnes et al. 1993).

These similarities strongly indicate that the presence of CYP26A1 is required to prevent the diffusion of RA from the RA-synthesizing regions of the trunk into the tissues of embryonic tail bud, perhaps to prevent premature exposure of its components to RA. *Raldh2* expression at E9–9.5 is adjacent to that of *Cyp26A1* in the posterior (presomitic and somitic) mesoderm, but is ex-

cluded from the tail bud (Fujii et al. 1997; Niederreither et al. 1997). Endogenous RA was detected in posterior somite explants, whereas tail-bud explants lacked detectable RA (Maden et al. 1998; Iulianella et al. 1999). Following embryonic RA administration, tail-bud explants have much higher RA-clearance ability than do posterior somite explants (Iulianella et al. 1999). We therefore postulate that *Cyp26A1* knockout results in an inability of tail-bud tissues to clear RA emanating from rostrally adjacent mesoderm, thus generating a local condition of "endogenous" RA teratogenicity, mimicking the effect of exogenously administered RA, which would overwhelm the clearance ability of CYP26A1 in the wild-type tail bud. Alterations of RA levels may represent an etiology for the human "caudal regression syndrome" that affects approximately 1/60,000 newborns and is reminiscent of the present murine phenotype (Padmanabhan et al. 1999). It is noteworthy that RARγ knockout mice are fully resistant to the RA-induced caudal axial truncations, indicating that this receptor is critically involved in these RA teratogenic effects (Lohnes et al. 1993). It will be interesting to see whether caudal abnormalities are less severe in double knockout mice lacking both CYP26A1 and RARγ.

Cyp26A1 *in vertebral and limb patterning*

Cyp26A1 mutants show abnormalities of cervical vertebrae, such that each mutant vertebra appeared to be posteriorly transformed into the likeness of its wild-type posterior neighbor. Anterior vertebral transformations have been observed in mouse RAR mutants (Lohnes et al. 1993, 1994), and posterior transformations have been seen after administration of excess RA to wild-type E7.5 embryos (Kessel and Gruss 1991). These RA-induced posterior transformations extended, however, to lumbosacral levels and also affected the occipital bones, resulting in the formation of a "proatlas" (Kessel and Gruss 1991), which is not found in *Cyp26A1*$^{-/-}$ mice. Thus, the lack of CYP26A1 function has less severe effects on vertebral patterning than does excess RA administration. Kessel and Gruss (1991) showed that the RA-induced transformations correlate with anterior shifts in the expression boundaries of several *Hox* genes. It has been shown largely through knockout or ectopic expression studies (Conlon 1995 and references therein), as well as through interspecific comparisons (Burke et al. 1995), that the combinatorial expression domains of *Hox* genes are responsible for the positioning of anatomical transitions between vertebrae. Interestingly, some of them are directly regulated via RA response elements (e.g., *Hoxa4, Hoxb4*, and *Hoxd4*, whose knockouts in the mouse generate transformations of cervical vertebrae) (Horan et al. 1994; Zhang et al. 1997). Lack of CYP26A1 function, affecting the normal distribution of endogenous RA levels, could interfere with the correct activation (and therefore the spatial extent) of *Hox* gene transcripts along the prevertebral column, thus leading to localized posterior transformations.

The localized distribution of RA in vertebrate limbs appears to be tightly controlled and application of exogenous retinoids can induce malformations (Kochhar and Aydelotte 1974; Eichele et al. 1985). The limbs of *Cyp26A1*$^{-/-}$ mutants appear normal, with the exception of the sirenomelic hindlimbs. Because *Cyp26A1* is expressed in limb buds (Fujii et al. 1997; Swindell et al. 1999), the lack of limb abnormalities in most of the null mutants indicates some functional redundancy. We have recently described another CYP26 subtype (CYP26B1/P450RAI-2) whose enzymatic activity on retinoids is indistinguishable from that of CYP26A1 (White et al. 2000b). *Cyp26B1* expression can be seen in distal limb bud mesenchyme at E9.5–11.5 embryos (G. MacLean and M. Petkovich, unpubl.), indicating that it could compensate for CYP26A1 deficiency during limb development. However, *Cyp26B1* is not expressed at detectable levels in the tail bud, and would thus not be expected to compensate for loss of CYP26A1 function in the development of posterior structures.

RA metabolism and hindbrain patterning

Cyp26A1 is transiently expressed during gastrulation in the anterior portion of the epiblast and neural plate, which are proposed to give rise to forebrain and midbrain territories (Fujii et al. 1997; Swindell et al. 1999). Spatially, this anterior domain is almost complementary to that of *Raldh2* in posterior and lateral mesoderm (Niederreither et al. 1997; Swindell et al. 1999), except for the presence of an intervening gap that may correspond to the prospective hindbrain region (see Fig. 10A; Swindell et al. 1999). This pattern of expression disappears before somitogenesis. *Cyp26A1* is then specifically expressed in r2 during the process of hindbrain segmentation (see Figs. 7A and 10B). At this stage, *Raldh2* is expressed in mesoderm up to the level of the posterior hindbrain (occipital somites). Both RALDH2 loss of function in mouse (Niederreither et al. 2000) and VAD in rats and quail (Maden et al. 1996; Gale et al. 1999; White et al. 2000a) result in specific abnormalities of the caudal hindbrain, in which the putative r4–r8 region was reduced and/or respecified ("transformed") toward a more anterior (r3- and r4-like) identity. Stepwise anteriorization of the caudal hindbrain was also observed following overexpression of *Cyp26A1* in Xenopus (Hollemann et al. 1998). In these studies, the rostral hindbrain (including r2), as well as other brain regions, did not seem to be affected.

Consistent with the idea that CYP26A1 acts to restrict the field of RA signaling, we found that *Cyp26A1*$^{-/-}$ mutants show patterning defects in a specific portion of the hindbrain, lying just rostrally to the region affected by retinoid deficiency. The overall rhombomeric organization of *Cyp26A1*$^{-/-}$ embryos appeared unaltered, indicating that its function is not required for proper hindbrain segmentation. Analysis of *Hoxb1* transcripts revealed, however, an anterior expansion of r4 size in mutants. Furthermore, ectopic *Hoxb1* expression was seen in patches in r3 and, sometimes, as a stripe in the caudal portion of r2, indicating a partial posterior transformation of these two rhombomeres into an r4-like character.

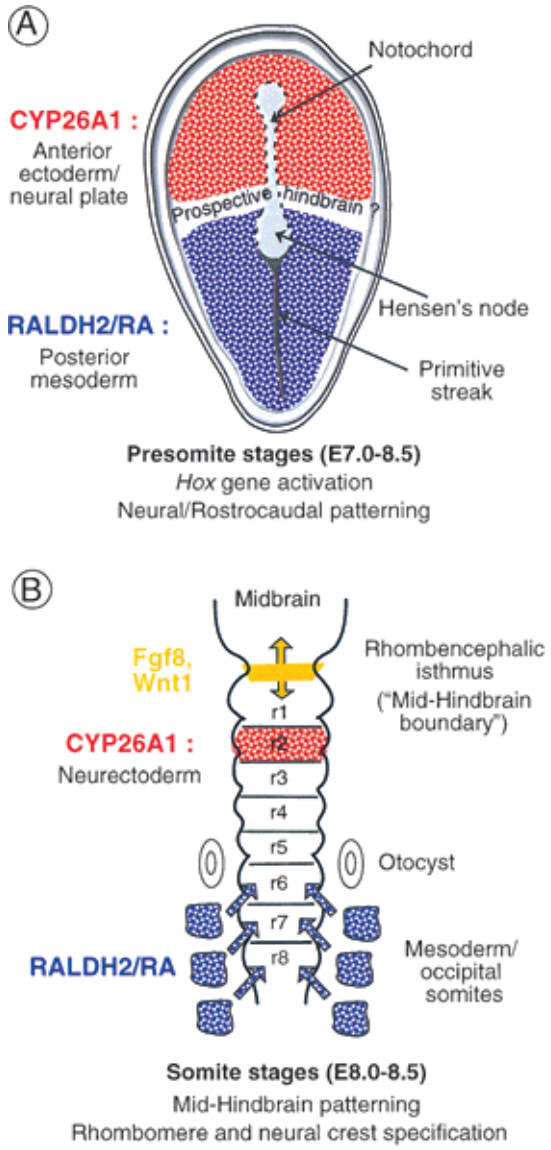

Figure 10. Schematic representation of the complementary RALDH2 retinoic acid (RA)-synthesizing and CYP26A1 RA-metabolizing activities during early embryo patterning (*A*) and hindbrain development (*B*). See the main text for references concerning the various expression patterns.

Down-regulation of *Meis2* in mutant r2 and abnormal *Mash1* transcript distribution in the caudal region of this rhombomere (mimicking an r4-characteristic pattern) further strengthen this conclusion. These patterning defects are clearly reminiscent of the effects of excess RA administration to E7.5–8 wild-type embryos, which leads to rostral expansion of *Hoxb1* expression at the expense of the *Krox20* r3 domain, or ectopic *Hoxb1* expression in r2 (Conlon 1995 and references therein). However, excess RA can lead to more drastic teratogenic effects, including lack of segmentation of the anterior hindbrain or severe head truncations, which have no counterpart in *Cyp26A1*$^{-/-}$ mutants, most likely because CYP26A1 knockout generates a condition of endogenous RA teratogenicity in only a very restricted hindbrain region (see following).

We therefore propose that *Cyp26A1* early expression in the rostral neural plate (Fig. 10A), and later in r2 (Fig. 10B), serves to precisely restrict the field of endogenous RA signaling within the developing hindbrain. Because the *Cyp26A1*$^{-/-}$ phenotypic defects arise well before completion of hindbrain segmentation (as seen by an early lack of restriction of the *EphA2* "pre-r4" domain in mutants) and are clearly not restricted to r2, we suggest that they result (at least in part) from a lack of early CYP26A1 activity in the rostral neural plate, which, therefore, would extend beyond forebrain and midbrain territories to the prospective rostral hindbrain. Embryonic RA produced by the mesoderm would signal through the plane of the neurectoderm to specify posterior rhombomere fate, in particular through the activation of "early" (3′-located) *Hox* genes, including *Hoxb1* (Fig. 10A; Gavalas and Krumlauf 2000). CYP26A1 activity, however, would be required to generate an RA-free domain in the rostral hindbrain region, thus defining (or sharpening) the rostral extent of *Hoxb1* expression and, therefore, the r3–r4 boundary. The later phase of *Cyp26A1* expression in r2 may reflect the fact that an RA-free environment has to be maintained in this rhombomere, either for its correct determination, or to prevent the posteriorizing RA signal from diffusing rostrally and counteracting the effects of signaling factors (e.g., FGF8 and Wnt1) derived from the rhombencephalic isthmus (Fig. 10B). These factors, which are required to generate a cerebellar fate (Joyner 1996), act during the phase of *Cyp26A1* r2-specific expression and some of them can be negatively regulated by RA in explant systems (Kolm et al. 1997). At the same stage, there is evidence that endogenous RA acts in the post-otic hindbrain: For instance, RARα/RARβ compound mutant mice (Dupé et al. 1999) show a rhombomeric phenotype distinct from that of *Raldh2*$^{-/-}$ mutants (Niederreither et al. 2000), indicating a later function of RA in patterning the r6–r8 region and its neural crest derivatives. It is noteworthy that the novel RA-metabolizing enzyme *Cyp26B1* shows no early expression equivalent to that of *Cyp26A1* in the rostral neural plate, but is specifically expressed in developing r5 and r6 (G. MacLean and M. Petkovich, unpubl.). Thus, *Cyp26B1* may perform a specific hindbrain function by modulating RA levels in these posterior rhombomeres.

Cyp26A1 *functions to define RA exclusion boundaries*

Several studies have proposed "anabolic" roles for CYP26A1, indicating that metabolites such as 4-oxo retinol or 4-oxo RA may have specialized activities in the regulation of cell growth or differentiation (Lane et al. 1999; Sonneveld et al. 1999; Ross et al. 2000). Thus some of the excess RA teratogenic effects occurring in *Cyp26A1*-expressing tissues may result from the abnormal production of such metabolites. In contrast, *Cyp26A1*$^{-/-}$ mutants, which cannot generate the 4-oxo metabolites, display a range of phenotypic defects that

all closely resemble those of excess RA administration. Thus, the present *Cyp26A1*$^{-/-}$ defects most probably result from accumulation of RA in regions that fail to express CYP26A1, arguing a "catabolic" role for this enzyme.

The often complementary patterns of *Raldh2* and *Cyp26A1* expression (Swindell et al. 1999) indicate that these enzymes might be involved in the generation of RA gradient(s), providing positional information for various embryonic structures. Whether such gradients actually exist will require the examination of RA distribution at the cellular level, by using sensitive RA-responsive reporter genes in wild-type and *Cyp26A1*$^{-/-}$ embryos. However, the expression patterns of RA-synthesizing enzymes (Niederreither et al. 1997; Moss et al. 1998; Swindell et al. 1999) and RA-responsive transgenes (e.g., Rossant et al. 1991) show sharply defined boundaries rather than graded expression patterns. Furthermore, *Raldh2*$^{-/-}$ mutants can be significantly rescued by maternally administered RA, which is not expected to form gradients in the embryo (Niederreither et al. 1999). This would indicate that RALDH2 (and other RA-synthesizing enzymes) functions to establish a requisite supply of RA to specific embryonic areas, not necessarily in a finely graded distribution. We posit that CYP26A1 acts to reduce RA to subthreshold levels, and therefore generate appropriate boundaries between regions that require RA signaling and those that have to be protected against its effects.

Materials and methods

Generation of Cyp26A1 *mutant mice*

A 15-kb *Cyp26A1* genomic clone was isolated from a mouse 129/Sv genomic library by using a full-length mouse *Cyp26A1* cDNA (Abu-Abed et al. 1998). *Cla*I and *Not*I restriction sites were generated in introns 1 and 6, respectively, by site-directed mutagenesis. Synthetic oligonucleotides containing an antisense *loxP* site and an upstream (5′) *Bgl*II restriction site were subcloned into the *Cla*I site in intron 1, and a *loxP*-flanked PGK-neo-poly(A) cassette, also containing an upstream (5′) *Bgl*II restriction site, was subcloned into the *Not*I site in intron 6. The 1.7-kb *Not*I fragment containing a *loxP*-flanked neomycin resistance gene under the control of the PGK promoter (L-PGK-neo-L cassette) was isolated from the pPGKneoA +LS1 plasmid, which was obtained by cloning the 1.7-kb *Bgl*II fragment isolated from pKJIB (Metzger et al. 1999) into the *Bam*HI site of a derivative of pLox2 (Sumi-Ichinose et al. 1997) containing a *Bgl*II and a *Not*I site between the *Sma*I and *Hin*dIII sites. The linearized targeting construct was electroporated into H1 ES cells as described (Dierich and Dollé 1997). Homologous recombination was identified by using 5′ and 3′ probes flanking the targeted region of *Cyp26A1*. This strategy was used in the subsequent genotyping of mouse tail and embryonic yolk sac genomic DNA. Yolk sac DNA was also genotyped by PCR with primers 5′-CTGGGCTGAAGGTGGGATAAGTGTCCTC-3′(P1), 5′-GGCGATGCTAGGTCTAGAGCTTTTCAAC-3′(P2), 5′-CCTGACCTGAGAATATTGCACGGAAGAC-3′(P3), and 5′-CCAAATGGAATGAAGCTGAACCGGGAAG-3′(P4), which amplify a 414-bp fragment from the wild-type allele and a 484-bp fragment from the null allele.

ES cells with one targeted allele (*Cyp26A1*$^{L3/+}$) were injected into C57BL/6 blastocysts, which were subsequently implanted into CD1 pseudo-pregnant females. Agouti males positive for germ-line transmission were mated with females constitutively expressing CMV-Cre (Dupé et al. 1997). Southern blotting was used to verify germ-line transmission in *Cyp26A1*$^{L3/+}$ mice and excision of exons 2–6 in their *Cyp26A1*$^{-/+}$ offspring.

Analyses of mouse embryos

Mouse embryos and fetuses were collected following natural overnight matings, fertilization being considered to take place around midnight. Histological stainings were performed after fixation in Bouin's fixative according to standard procedures (Mark et al. 1993). Whole-mount alcian blue skeletal stainings were performed as described (Jegalian and De Robertis 1992). Whole-mount in situ hybridization with digoxigenin-labeled probes was performed as described (Decimo et al. 1995) by using template plasmids kindly provided by P. Charnay (*Krox20*), F. Guillemot (*Mash1*), B. Herrmann (*Brachyury*), A. Joyner (*En2*), R. Krumlauf (*Hoxb1*), A.P. McMahon (*Wnt3a*), and D. Wilkinson (*EphA2*). The TUNEL and antineurofilament staining procedures were described in Conlon et al. (1995) and Mark et al. (1993), respectively.

Acknowledgments

We thank A. Dierich for the ES cell line; M. Le Meur and E. Metzger for supervising animal care; and J-M. Bornert, V. Fraulob, J-F. Kleinmann, B. Schuhbaur, C. Wood, and N. Cabilio for expert technical assistance. We also thank D. Lohnes, C. Mendelsohn, and A. Iulianella for useful discussions. This work was supported by grants from the Canadian Institutes of Health Research and the National Cancer Institute of Canada (laboratory of M.P.) and by funds from the Centre National de la Recherche Scientifique, Institut National de la Santé et de la Recherche Médicale, CollÈge de France, HÔpitaux Universitaires de Strasbourg, Association pour la Recherche sur le Cancer, Fondation pour la Recherche Médicale and MinistÈre de l'Éducation Nationale, de la Recherche et de la Technologie (laboratory of P.C.). S.A. is a recipient of a Medical Research Council of Canada Studentship award.

The publication costs of this article were defrayed in part by payment of page charges. This article must therefore be hereby marked "advertisement" in accordance with 18 USC section 1734 solely to indicate this fact.

References

Abu-Abed, S.S., Beckett, B.R., Chiba, H., Chithalen, J.V., Jones, G., Metzger, D., Chambon, P., and Petkovich, M. 1998. Mouse P450RAI (CYP26) expression and retinoic acid-inducible retinoic acid metabolism in F9 cells are regulated by retinoic acid receptor γ and retinoid X receptor α. *J. Biol. Chem.* **273:** 2409–2415.

Burke, A.C., Nelson, C.E., Morgan, B.A., and Tabin, C. 1995. Hox genes and the evolution of vertebrate axial morphology. *Development* **121:** 333–346.

Chambon, P. 1996. A decade of molecular biology of retinoic acid receptors. *FASEB J.* **10:** 940–954.

Chazaud, C., Chambon, P., and Dollé, P. 1999. Retinoic acid is required in the mouse embryo for left-right asymmetry determination and heart morphogenesis. *Development* **126:** 2589–2596.

Conlon, R.A. 1995. Retinoic acid and pattern formation in vertebrates. *Trends Genet.* **11:** 314–319.

Conlon, R.A., Reaume, A.G., and Rossant, J. 1995. Notch1 is required for the coordinate segmentation of somites. *Development* **121:** 1533–1545.

Davenne, M., Maconochie, M.K., Neun, R., Pattyn, A., Chambon, P., Krumlauf, R., and Rijli, F.M. 1999. Hoxa2 and Hoxb2 control dorsoventral patterns of neuronal development in the rostral hindbrain. *Neuron* **22:** 677–691.

Decimo, D., Georges-Labouesse, E., and Dolle, P. 1995. In situ hybridization to cellular RNA. In *Gene probes 2: A practical approach* (eds. B.D. James and S.J. Higgins). Oxford University Press, New York.

Dierich, A. and Dollé, P. 1997. Gene targeting in embryonic stem cells. In *Methods in developmental toxicology and biology* (eds. S. Klug and T. Theil), pp. 111–123. Blackwell Science.

Duester, G. 2000. Families of retinoid dehydrogenases regulating vitamin A function: Production of visual pigment and retinoic acid. *Eur. J. Biochem.* **267:** 4315–4324.

Dupé, V., Davenne, M., Brocard, J., Dolle, P., Mark, M., Dierich, A., Chambon, P., and Rijli, F.M. 1997. In vivo functional analysis of the Hoxa-1 3′ retinoic acid response element (3′RARE). *Development* **124:** 399–410.

Dupé, V., Ghyselinck, N.B., Wendling, O., Chambon, P., and Mark, M. 1999. Key roles of retinoic acid receptors α and β in the patterning of the caudal hindbrain, pharyngeal arches and otocyst in the mouse. *Development* **126:** 5051–5059.

Eichele, G., Tickle, C., and Alberts, B.M. 1985. Studies on the mechanism of retinoid-induced pattern duplications in the early chick limb bud: temporal and spatial aspects. *J. Cell. Biol.* **101:** 1913–1920.

Fujii, H., Sato, T., Kaneko, S., Gotoh, O., Fujii-Kuriyama, Y., Osawa, K., Kato, S., and Hamada, H. 1997. Metabolic inactivation of retinoic acid by a novel P450 differentially expressed in developing mouse embryos. *EMBO J.* **16:** 4163–4173.

Gale, E., Zile, M., and Maden, M. 1999. Hindbrain respecification in the retinoid-deficient quail. *Mech. Dev.* **89:** 43–54.

Gavalas, A. and Krumlauf, R. 2000. Retinoid signalling and hindbrain patterning. *Curr. Opin. Genet. Dev.* **10:** 380–386.

Guillemot, F. and Joyner, A.L. 1993. Dynamic expression of the murine Achaete-Scute homologue Mash-1 in the developing nervous system. *Mech. Dev.* **42:** 171–185.

Hofmann, C. and Eichele, G. 1994. Retinoids in development. In *The Retinoids: Biology, Chemistry, and Medicine* (eds. M.B. Sporn, A.B. Roberts, and D.S. Goodman), pp. 387–441. Raven Press, New York.

Hollemann, T., Chen, Y., Grunz, H., and Pieler, T. 1998. Regionalized metabolic activity establishes boundaries of retinoic acid signalling. *EMBO J.* **17:** 7361–7372.

Horan, G.S., Wu, K., Wolgemuth, D.J., and Behringer, R.R. 1994. Homeotic transformation of cervical vertebrae in Hoxa-4 mutant mice. *Proc. Natl. Acad. Sci.* **91:** 12644–12648.

Iulianella, A., Beckett, B., Petkovich, M., and Lohnes, D. 1999. A molecular basis for retinoic acid-induced axial truncation. *Dev. Biol.* **205:** 33–48.

Jegalian, B.G. and De Robertis, E.M. 1992. Homeotic transformations in the mouse induced by overexpression of a human Hox3.3 transgene. *Cell* **71:** 901–910.

Joyner, A.L. 1996. Engrailed, Wnt and Pax genes regulate midbrain–hindbrain development. *Trends Genet.* **12:** 15–20.

Kastner, P., Mark, M., Ghyselinck, N., Krezel, W., Dupe, V., Grondona, J.M., and Chambon, P. 1997. Genetic evidence that the retinoid signal is transduced by heterodimeric RXR/RAR functional units during mouse development. *Development* **124:** 313–26.

Kessel, M. 1992. Respecification of vertebral identities by retinoic acid. *Development* **115:** 487–501.

Kessel, M. and Gruss, P. 1991. Homeotic transformations of murine vertebrae and concomitant alteration of Hox codes induced by retinoic acid. *Cell* **67:** 89–104.

Kochhar, D.M. 1973. Limb development in mouse embryos. I. Analysis of teratogenic effects of retinoic acid. *Teratology* **7:** 289–298.

Kochhar, D.M. and Aydelotte, M.B. 1974. Susceptible stages and abnormal morphogenesis in the developing mouse limb, analysed in organ culture after transplacental exposure to vitamin A (retinoic acid). *J. Embryol. Exp. Morphol.* **31:** 721–734.

Kolm, P.J., Apekin, V., and Sive, H. 1997. Xenopus hindbrain patterning requires retinoid signaling. *Dev. Biol.* **192:** 1–16.

Krumlauf, R. 1994. Hox genes in vertebrate development. *Cell* **78:** 191–201.

Lane, M.A., Chen, A.C., Roman, S.D., Derguini, F., and Gudas, L.J. 1999. Removal of LIF (leukemia inhibitory factor) results in increased vitamin A (retinol) metabolism to 4-oxoretinol in embryonic stem cells. *Proc. Natl. Acad. Sci.* **96:** 13524–13529.

Lohnes, D., Kastner, P., Dierich, A., Mark, M., LeMeur, M., and Chambon, P. 1993. Function of retinoic acid receptor γ in the mouse. *Cell* **73:** 643–658.

Lohnes, D., Mark, M., Mendelsohn, C., Dolle, P., Dierich, A., Gorry, P., Gansmuller, A., and Chambon, P. 1994. Function of the retinoic acid receptors (RARs) during development (I). Craniofacial and skeletal abnormalities in RAR double mutants. *Development* **120:** 2723–2748.

Maden, M. 1999. Heads or tails? Retinoic acid will decide. *Bioessays* **21:** 809–812.

Maden, M., Gale, E., Kostetskii, I., and Zile, M. 1996. Vitamin A-deficient quail embryos have half a hindbrain and other neural defects. *Curr. Biol.* **6:** 417–426.

Maden, M., Sonneveld, E., van der Saag, P.T., and Gale, E. 1998. The distribution of endogenous retinoic acid in the chick embryo: Implications for developmental mechanisms. *Development* **125:** 4133–4144.

Mark, M., Lufkin, T., Vonesch, J.L., Ruberte, E., Olivo, J.C., Dolle, P., Gorry, P., Lumsden, A., and Chambon, P. 1993. Two rhombomeres are altered in Hoxa-1 mutant mice. *Development* **119:** 319–338.

Mascrez, B., Mark, M., Dierich, A., Ghyselinck, N.B., Kastner, P., and Chambon, P. 1998. The RXRα ligand-dependent activation function 2 (AF-2) is important for mouse development. *Development* **125:** 4691–4707.

McCaffery, P., Wagner, E., O'Neil, J., Petkovich, M., and Drager, U.C. 1999. Dorsal and ventral rentinoic territories defined by retinoic acid synthesis, break-down and nuclear receptor expression. *Mech. Dev.* **85:** 203–214.

Mendelsohn, C., Ruberte, E., LeMeur, M., Morriss-Kay, G., and Chambon, P. 1991. Developmental analysis of the retinoic acid-inducible RAR-β 2 promoter in transgenic animals. *Development* **113:** 723–734.

Mendelsohn, C., Lohnes, D., Decimo, D., Lufkin, T., LeMeur, M., Chambon, P., and Mark, M. 1994. Function of the retinoic acid receptors (RARs) during development (II). Multiple abnormalities at various stages of organogenesis in RAR double mutants. *Development* **120:** 2749–2771.

Metzger, D., Scheer, E., Soldatov, A., and Tora, L. 1999. Mammalian TAF(II)30 is required for cell cycle progression and specific cellular differentiation programmes. *EMBO J.* **18:** 4823–4834.

Morriss-Kay, G.M. and Sokolova, N. 1996. Embryonic development and pattern formation. *FASEB J.* **10:** 961–968.

Moss, J.B., Xavier-Neto, J., Shapiro, M.D., Nayeem, S.M., McCaffery, P., Drager, U.C., and Rosenthal, N. 1998. Dynamic patterns of retinoic acid synthesis and response in the developing mammalian heart. *Dev. Biol.* **199:** 55–71.

Niederreither, K., McCaffery, P., Drager, U.C., Chambon, P., and Dolle, P. 1997. Restricted expression and retinoic acid-induced downregulation of the retinaldehyde dehydrogenase type 2 (RALDH-2) gene during mouse development. *Mech. Dev.* **62:** 67–78.

Niederreither, K., Subbarayan, V., Dolle, P., and Chambon, P. 1999. Embryonic retinoic acid synthesis is essential for early mouse post- implantation development. *Nat. Genet.* **21:** 444–448.

Niederreither, K., Vermot, J., Schuhbaur, B., Chambon, P., and Dolle, P. 2000. Retinoic acid synthesis and hindbrain patterning in the mouse embryo. *Development* **127:** 75–85.

Oulad-Abdelghani, M., Chazaud, C., Bouillet, P., Mattei, M.G., Dolle, P., and Chambon, P. 1998. Stra3/lefty, a retinoic acid-inducible novel member of the transforming growth factor-β superfamily. *Int. J. Dev. Biol.* **42:** 23–32.

Padmanabhan, R. 1998. Retinoic acid-induced caudal regression syndrome in the mouse fetus. *Reprod. Toxicol.* **12:** 139–151.

Padmanabhan, R., Naruse, I., and Shiota, K. 1999. Caudal dysgenesis in staged human embryos: Carnegie stages 16–23. *Am. J. Med. Genet.* **87:** 115–127.

Ray, W.J., Bain, G., Yao, M., and Gottlieb, D.I. 1997. CYP26, a novel mammalian cytochrome P450, is induced by retinoic acid and defines a new family. *J. Biol. Chem.* **272:** 18702–18708.

Ross, S.A., McCaffery, P.J., Drager, U.C., and De Luca, L.M. 2000. Retinoids in embryonal development. *Physiol. Rev.* **80:** 1021–1054.

Rossant, J., Zirngibl, R., Cado, D., Shago, M., and Giguere, V. 1991. Expression of a retinoic acid response element-hsplacZ transgene defines specific domains of transcriptional activity during mouse embryogenesis. *Genes & Dev.* **5:** 1333–1344.

Sakai, Y., Meno, C., Fujii, H., Nishino, J., Saijoh, Y., Rossant, J., and Hamada, H. 2001. The retinoic acid-inactivating enzyme CYP26 is essential for establishing a graded distribution of retinoic acid along the anterio-posterior axis within the mouse embryo. *Genes & Dev.* **15:** 213–225.

Schneider-Maunoury, S., Topilko, P., Seitandou, T., Levi, G., Cohen-Tannoudji, M., Pournin, S., Babinet, C., and Charnay, P. 1993. Disruption of Krox-20 results in alteration of rhombomeres 3 and 5 in the developing hindbrain. *Cell* **75:** 1199–1214.

Shum, A.S., Poon, L.L., Tang, W.W., Koide, T., Chan, B.W., Leung, Y.C., Shiroishi, T., and Copp, A.J. 1999. Retinoic acid induces down-regulation of Wnt-3a, apoptosis and diversion of tail-bud cells to a neural fate in the mouse embryo. *Mech. Dev.* **84:** 17–30.

Sonneveld, E., van den Brink, C.E., Tertoolen, L.G., van der Burg, B., and van der Saag, P.T. 1999. Retinoic acid hydroxylase (CYP26) is a key enzyme in neuronal differentiation of embryonal carcinoma cells. *Dev. Biol.* **213:** 390–404.

Sumi-Ichinose, C., Ichinose, H., Metzger, D., and Chambon, P. 1997. SNF2β-BRG1 is essential for the viability of F9 murine embryonal carcinoma cells. *Mol. Cell. Biol.* **17:** 5976–5986.

Swindell, E.C., Thaller, C., Sockanathan, S., Petkovich, M., Jessell, T.M., and Eichele, G. 1999. Complementary domains of retinoic acid production and degradation in the early chick embryo. *Dev. Biol.* **216:** 282–296.

Takada, S., Stark, K.L., Shea, M.J., Vassileva, G., McMahon, J.A., and McMahon, A.P. 1994. Wnt-3a regulates somite and tailbud formation in the mouse embryo. *Genes & Dev.* **8:** 174–189.

White, J.A., Guo, Y.D., Baetz, K., Beckett-Jones, B., Bonasoro, J., Hsu, K.E., Dilworth, F.J., Jones, G., and Petkovich, M. 1996. Identification of the retinoic acid-inducible all-trans-retinoic acid 4–hydroxylase. *J. Biol. Chem.* **271:** 29922–29927.

White, J.A., Beckett-Jones, B., Guo, Y.D., Dilworth, F.J., Bonasoro, J., Jones, G., and Petkovich, M. 1997. cDNA cloning of human retinoic acid-metabolizing enzyme (hP450RAI) identifies a novel family of cytochromes P450. *J. Biol. Chem.* **272:** 18538–18541.

White, J.A., Ramshaw, H., Taimi, M., Stangle, W., Zhang, A., Everingham, S., Creighton, S., Tam, S.P., Jones, G., and Petkovich, M. 2000a. Identification of the human cytochrome P450, P450RAI-2, which is predominantly expressed in the adult cerebellum and is responsible for all-trans-retinoic acid metabolism. *Proc. Natl. Acad. Sci.* **97:** 6403–6648.

White, J.C., Highland, M., Kaiser, M., and Clagett-Dame, M. 2000b. Vitamin A deficiency results in the dose-dependent acquisition of anterior character and shortening of the caudal hindbrain of the rat embryo. *Dev. Biol.* **220:** 263–284.

Wilkinson, D.G., Bhatt, S., and Herrmann, B.G. 1990. Expression pattern of the mouse T gene and its role in mesoderm formation. *Nature* **343:** : 657–659.

Xu, Q., Mellitzer, G., Robinson, V., and Wilkinson, D.G. 1999. In vivo cell sorting in complementary segmental domains mediated by Eph receptors and ephrins. *Nature* **399:** 267–271.

Zhang, F., Popperl, H., Morrison, A., Kovacs, E.N., Prideaux, V., Schwarz, L., Krumlauf, R., Rossant, J., and Featherstone, M.S. 1997. Elements both 5′ and 3′ to the murine Hoxd4 gene establish anterior borders of expression in mesoderm and neurectoderm. *Mech. Dev.* **67:** 49–58.